

# CrystEngComm

Accepted Manuscript



This is an *Accepted Manuscript*, which has been through the Royal Society of Chemistry peer review process and has been accepted for publication.

*Accepted Manuscripts* are published online shortly after acceptance, before technical editing, formatting and proof reading. Using this free service, authors can make their results available to the community, in citable form, before we publish the edited article. We will replace this *Accepted Manuscript* with the edited and formatted *Advance Article* as soon as it is available.

You can find more information about *Accepted Manuscripts* in the [Information for Authors](#).

Please note that technical editing may introduce minor changes to the text and/or graphics, which may alter content. The journal's standard [Terms & Conditions](#) and the [Ethical guidelines](#) still apply. In no event shall the Royal Society of Chemistry be held responsible for any errors or omissions in this *Accepted Manuscript* or any consequences arising from the use of any information it contains.

## ARTICLE

# In-situ synthesis of porous ZnO-embedded $Zn_{1-x}Cd_xS/CdS$ heterostructure for the enhanced photocatalytic activity

Cite this: DOI: 10.1039/x0xx00000x

Received 00th January 2012,  
Accepted 00th January 2012

DOI: 10.1039/x0xx00000x

[www.rsc.org/](http://www.rsc.org/)

Rong Chen, Kui Li, Xiao-Shu Zhu, Shuai-Lei Xie, Long-Zhang Dong, Shun-Li Li\* and Ya-Qian Lan\*

The in-situ synthesis of ZnO-embedded  $Zn_{1-x}Cd_xS/CdS$  heterostructure nanocrystals were achieved using a simple surfactant-free hydrothermal route. The morphology and the content of exposed active sites of  $Zn_{1-x}Cd_xS/CdS$  could be facilely modulated by varying the particle size of ZnS precursors, and the heterostructure with the smallest particle size showed the largest photocatalytic activity of 22.99 mmol/h/g in  $Na_2S + Na_2SO_3$  solution. Furthermore, the in-situ embedding of ZnO cocatalyst on the  $Zn_{1-x}Cd_xS/CdS$  heterostructure dramatically improved its photocatalytic activity to 84.17 mmol/h/g, which is 765 times higher than that of CdS prepared by hydrothermal method. More significantly, the ZnO-embedded  $Zn_{1-x}Cd_xS/CdS$  heterostructure gave considerable  $H_2$ -production rate even in the absence of hole scavenger, although the bare  $Zn_{1-x}Cd_xS/CdS$  exhibited no hydrogen evolution, and it showed very competitive photocatalytic activity in methanol in comparison with that in  $Na_2S + Na_2SO_3$  solution under the similarly alkaline circumstance. These investigations indicate that the existence of ZnO cocatalyst in the heterostructure could not only effectively improve the photocatalytic activity by suppressing the recombination of charge carriers and acting as photocatalytic reaction sites, but also make it possible to adopt methanol as the sacrificial reagent for sulfide photocatalyst.

## Introduction

Semiconductor nanocrystals have attracted much attention in the areas of photocatalysis,<sup>1</sup> and photoelectrochemistry (PEC)<sup>2</sup> owing to their excellent photocatalytic and photoelectronic properties.<sup>3</sup> However, the limited visible light absorption and rapid recombination of photo-generated charge carriers in semiconductor photocatalysts restrict their practical applications.<sup>4</sup> Fabricating the sulfide heterostructure not only facilitates the separation of charge carriers,<sup>5</sup> but also improves the visible light absorption due to their narrow band gap.<sup>6</sup> However, the preparation of sulfide heterostructures usually involves complex routes by loading one semiconductor on the other one, which needs precise control of synthetic parameters in each step.<sup>7</sup> This method not only limits the scale-up synthesis of heterostructure,<sup>5</sup> but also induces the formation of interfacial problems.<sup>8</sup> Moreover, the surface based characteristic of photocatalytic water splitting reaction makes the content of exposed active sites an important factor in the design of high-performance heterostructure photocatalyst. The organic surfactants were extensively adopted to modulate the morphology of the nanomaterials. Whereas, the surfactants inevitably contaminate the heterostructures, and may

substantially impair the performance of the heterostructures.<sup>9</sup> Therefore, searching for an efficient surfactant-free hydrothermal method for the in-situ synthesis of sulfide heterostructure with improved amount of active sites is an important subject from both theoretical and practical viewpoints.

Cocatalysts, such as graphene, Pt, NiO and  $MoS_2$  could facilitate the separation of photo-excited holes/electrons pairs, and/or act as  $H_2$ -production sites.<sup>10</sup> ZnO was widely used as photocatalyst due to its high electron mobility and long photo-excited lifetime.<sup>11</sup> Notably, it was extensively demonstrated that the oxygen vacancies in ZnO could work as electron traps to accept electrons and inhibit the recombination of charge carriers.<sup>12</sup> The oxygen vacancies in ZnO could also act as the favored sites for catalyzing the N-formylation reaction as reported by Zhu's group.<sup>13</sup> Furthermore, it was demonstrated in Zong's investigation that the ZnO could function as cocatalyst for improving the catalytic activity of combined reforming-hydrogenolysis of glycerol.<sup>14</sup> These unique features of ZnO make it an excellent cocatalyst for improving the photocatalytic activity of sulfide photocatalysts. On the other hand, it is well known that the sulfide photocatalysts show an excellent

photocatalytic activity only in the  $\text{Na}_2\text{S} + \text{Na}_2\text{SO}_3$  sacrificial solution, which is toxic and not stable in the air condition.<sup>15</sup> Unfortunately, the sulfide photocatalysts give the negligible photocatalytic activity in the widely used hole scavenger, such as methanol.<sup>16</sup> If we could fabricate the hetero-nanomaterial composed by ZnO and sulfide heterostructure, we can simultaneously take the advantages of the two components for photocatalytic water splitting.<sup>17</sup> This material maybe not only improve the photocatalytic activity of sulfide photocatalysts in the traditional  $\text{Na}_2\text{S} + \text{Na}_2\text{SO}_3$  solution, but also make it possible for the utilization of methanol solution as sacrificial reagent for sulfide photocatalysts. Up to date, both the fabrication of fine grained ZnO-embedded sulfide heterostructure and efficient method for improving the photocatalytic activity in methanol sacrificial solution were scarcely reported.

In view of the aforementioned ideas, we select  $\text{Zn}_{1-x}\text{Cd}_x\text{S}/\text{CdS}$  as the sulfide heterostructure to synthesize ZnO-embedded fine-grained  $\text{Zn}_{1-x}\text{Cd}_x\text{S}/\text{CdS}$  heterostructure using a surfactant-free hydrothermal method based on the following points: i)  $\text{Zn}_{1-x}\text{Cd}_x\text{S}/\text{CdS}$  shows improved structure matching and photocatalytic performance due to the tunable parameters, and the excellent photocatalytic activity of  $\text{Zn}_{1-x}\text{Cd}_x\text{S}$ ;<sup>18</sup> ii) ZnS precursors with different morphologies were prepared by changing the concentrations of NaOH, and the content of exposed active sites of the  $\text{Zn}_{1-x}\text{Cd}_x\text{S}/\text{CdS}$  heterostructure could be facily modulated by the varied particle sizes of ZnS precursors; iii) the in-situ embedding of the well-dispersed ZnO nanocrystals on the  $\text{Zn}_{1-x}\text{Cd}_x\text{S}/\text{CdS}$  heterostructure was obtained by the reaction between  $\text{OH}^-$  and the residual  $\text{Zn}^{2+}$  derived from the cation exchange of ZnS with  $\text{Cd}^{2+}$ .

Herein, the  $\text{Zn}_{1-x}\text{Cd}_x\text{S}/\text{CdS}$  heterostructures with modulated morphologies were facily fabricated through varying the particle sizes of ZnS precursors by the implantation of  $\text{OH}^-$  on their surfaces. The photocatalytic activity of  $\text{Zn}_{1-x}\text{Cd}_x\text{S}/\text{CdS}$  heterostructure was found closely dependent on the exposed active sites, and the heterostructure with the smallest particle size shows the maximal  $\text{H}_2$ -evolution activity of 22.99 mmol/h/g. The in-situ synthesis of ZnO-embedded  $\text{Zn}_{1-x}\text{Cd}_x\text{S}/\text{CdS}$  heterostructure was obtained by introducing different contents of NaOH. The ZnO nanocrystal, serving as cocatalyst to separate the charge carriers and acting as  $\text{H}_2$ -production sites, shows tremendous enhancement on the photocatalytic activity of  $\text{Zn}_{1-x}\text{Cd}_x\text{S}/\text{CdS}$  heterostructure to 84.17 mmol/h/g, especially in the methanol solution. Notably, the ZnO-embedded  $\text{Zn}_{1-x}\text{Cd}_x\text{S}/\text{CdS}$  shows distinct photocatalytic  $\text{H}_2$ -production of 0.18 mmol/h/g even in the absence of sacrificial agent, although the  $\text{Zn}_{1-x}\text{Cd}_x\text{S}/\text{CdS}$  shows no hydrogen production. The content of exposed active sites and the loading of ZnO cocatalyst on the heterojunction show synergistic effect on the photocatalytic  $\text{H}_2$ -evolution activity.

## Experimental section

### Materials

Cadmium nitrate tetrahydrate ( $\text{Cd}(\text{NO}_3)_2 \cdot 4\text{H}_2\text{O}$ ), zinc chloride ( $\text{ZnCl}_2$ ), thiourea ( $\text{CH}_4\text{N}_2\text{S}$ ) and sodium hydroxide (NaOH) are analytical grade, and used as received without further purification.

### Synthesis of ZnS precursors with different particle sizes

The ZnS precursors were prepared using  $\text{ZnCl}_2$ ,  $\text{CH}_4\text{N}_2\text{S}$  as Zn, S sources via a hydrothermal method. NaOH was adopted to modulate the particle size of ZnS. In a typical process, 3.0 mmol  $\text{ZnCl}_2$  and 6.0 mmol  $\text{CH}_4\text{N}_2\text{S}$  were dissolved in 25 mL distilled water (solution A). Different contents of NaOH with the molar ratios of NaOH/Zn equaling to 0, 1, 2, 4, 8, 10, 20 were dissolved in 5 mL distilled water (solution B). Then the solution B was added into solution A slowly under ultrasound for 0.5 h. The resultant solution was subsequently transferred into 50 mL teflon-lined autoclave and maintained 180 °C for 21 h. The final white products were rinsed three times with distilled water and ethanol respectively, and dried at 60 °C for overnight in a vacuum oven to evaporate the solvent. The obtained ZnS nanocrystals with different particle size were used as precursor for the fabrication of the heterostructure samples.

### Synthesis of the heterostructure samples with modulated morphology by the different particle size of ZnS precursors

30 mg ZnS precursors (prepared with the molar ratios of NaOH/Zn = 0, 1, 2, 4, 8, 10, 20) were dissolved in 10 mL deionized water under ultrasound for a few minutes. Suitable content of  $\text{Cd}(\text{NO}_3)_2 \cdot 4\text{H}_2\text{O}$  ( $\text{Cd}/(\text{Zn}+\text{Cd}) = 30$  at%) were dissolved in deionized water (2.8 mL) and then drop into the aforementioned solution quickly under mild stirring. After several minutes, the obtained solution was transferred into 15 mL autoclave and maintained 140 °C for 12 h. The final products were rinsed with distilled deionized water and ethanol for three times, respectively, and dried at 60 °C overnight in the vacuum oven to evaporate the solvent.

### In-situ synthesis of the ZnO cocatalyst

30 mg ZnS with the smallest particle size (prepared with the NaOH/Zn molar ratio of 4) was dissolved in 8 mL deionized water under ultrasound for a few minutes (Solution A). Suitable content of  $\text{Cd}(\text{NO}_3)_2 \cdot 4\text{H}_2\text{O}$  ( $\text{Cd}/(\text{Zn}+\text{Cd}) = 30$  at%) was dissolved in deionized water (3 mL) (Solution B). Different contents of NaOH with the ratio of NaOH/Cd equaling to 1, 5, 10, 15 and 20 were dissolved in 1 mL distilled water and then dropped into the mixture solutions of A+B quickly under mild stirring. After several minutes, the obtained solution was transferred into 15 mL autoclave and maintained 140 °C for 12 h. The final yellow products were rinsed with distilled deionized water and ethanol for three times respectively, and dried at 60 °C overnight in the vacuum oven to evaporate the solvent.

## Characterization

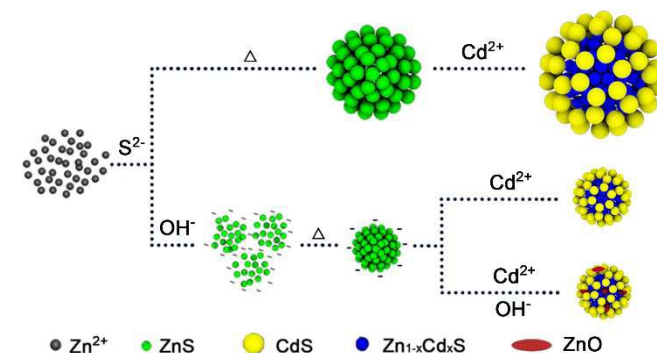
The powder X-ray diffraction (XRD) patterns were recorded on a D/max 2500 VL/PC diffractometer (Japan) equipped with graphite monochromatized Cu K $\alpha$  radiation ( $\lambda = 1.54060 \text{ \AA}$ ). Corresponding work voltage and current is 40 kV and 100 mA, respectively. The transmission electron microscopy (TEM) and high-resolution TEM (HRTEM) images were recorded on JEOL-2100F apparatus at an accelerating voltage of 200 kV. Surface morphologies of the heterojunction materials were examined by a scanning electron microscope (SEM, JSM-7600F) at an acceleration voltage of 10 kV. The energy-dispersive X-ray spectroscopy (EDX) was taken on JSM-5160LV-Vantage typed energy spectrometer. UV-visible diffused reflectance spectra was recorded using a Cary 5000 UV-Vis spectrometer (Viarian, USA) with BaSO<sub>4</sub> as a reflectance standard. The Brunauer–Emmett–Teller (BET) specific surface area ( $S_{\text{BET}}$ ), nitrogen adsorption of the heterojunction samples were analyzed by an Autosorb-iQ adsorption apparatus (Quantachrome instruments, USA). All of the samples were degassed at 90 °C for 3 hours prior to nitrogen adsorption measurements. The  $S_{\text{BET}}$  was determined by a multipoint BET method using adsorption data in the relative pressure ( $P/P_0$ ) range of 0.05 – 0.3. Electrochemical impedance spectra (EIS) measurements were carried out in three-electrode system and recorded over a frequency range of 500 kHz-200 MHz with ac amplitude of 10 mV at 0.5 V. Na<sub>2</sub>S (0.1 M) and Na<sub>2</sub>SO<sub>3</sub> (0.02 M) mixture solution was used as the supporting electrolyte. EIS data were recorded using Electrochemical workstation (EC-lab, SP-150, VMP3-based instruments, America) under a surface power density of about 0.1 mW/cm<sup>2</sup>. Raman spectra of powder samples were obtained on Lab-RAM HR800 with a laser excitation wavelength of 514.5 nm.

## Photocatalytic Hydrogen Production

The photocatalytic H<sub>2</sub>-production experiments were performed via a photocatalytic H<sub>2</sub>-production activity evaluation system (CEL-SPH2N, CEALight, China) in a 300 mL Pyrex flask, and the openings of the flask were sealed with silicone rubber septum. A 300 W xenon arc lamp through a UV-cutoff filter with a wavelength range of 420–1000 nm, which was positioned 13 cm away from the reaction solution, was used as a visible light source to trigger the photocatalytic reaction. The focused intensity on the flask was  $\sim 200 \text{ mW}\cdot\text{cm}^{-2}$ , which was measured by a FZ-A visible-light radiometer (CEL-SPH2N, CEALight, China). In a typical photocatalytic H<sub>2</sub>-production experiment, 5 mg of the as-prepared photocatalyst was suspended in 100 mL of mixed aqueous solution containing Na<sub>2</sub>S (0.35 M) and Na<sub>2</sub>SO<sub>3</sub> (0.25 M). Before irradiation, the system was vacuumed for 5 min via the vacuum pump to completely remove the dissolved oxygen and ensure the reactor was in an anaerobic condition. A continuous magnetic stirrer was applied at the bottom of the reactor to keep the photocatalyst particles in suspension during the experiments. H<sub>2</sub>

content was analyzed by gas chromatography (GC-7900, CEALight, China). All glasswares were carefully rinsed with distilled water prior to usage.

## Results and discussion



**Scheme 1.** Schematic illustrations of the fabrication of ZnS precursors, Zn<sub>1-x</sub>Cd<sub>x</sub>S/CdS heterostructure with modulated morphology, and the ZnO-embedded Zn<sub>1-x</sub>Cd<sub>x</sub>S/CdS heterostructure.

Zn<sub>1-x</sub>Cd<sub>x</sub>S/CdS heterostructures with adjustable morphologies were accessible by varying the particle sizes of ZnS precursors.<sup>19</sup> Scheme 1 illustrates the fabrication route for modulating the morphologies of ZnS precursors, the Zn<sub>1-x</sub>Cd<sub>x</sub>S/CdS heterostructure and ZnO-embedded Zn<sub>1-x</sub>Cd<sub>x</sub>S/CdS heterostructure. The ZnS precursors possessing different particle sizes were firstly fabricated, where the hydroxide plays an indispensable role in the formation of the fine-grained ZnS precursor by the repulsive interaction among ZnS nanoparticles.<sup>20</sup>

The morphologies of Zn<sub>1-x</sub>Cd<sub>x</sub>S/CdS heterostructures with the optimal content of Cd could be facily modulated by the different particle sizes of ZnS precursors (Fig. S1).<sup>21</sup> The Zn<sup>2+</sup> derived from the cation exchange between ZnS and Cd<sup>2+</sup> reacted with the superfluous hydroxyl ion and produced [Zn(OH)<sub>4</sub>]<sup>2-</sup>, then immediately transformed into the ZnO,<sup>22</sup> and the ZnO-embedded Zn<sub>1-x</sub>Cd<sub>x</sub>S/CdS heterostructure was formed. The Zn<sub>1-x</sub>Cd<sub>x</sub>S/CdS heterostructure samples derived from the ZnS precursors with different particle sizes were abbreviated as ZAC<sub>m</sub> ( $m = 0, 1, 2, 4, 10, 20$ ,  $m$  equals to the molar ratio of NaOH/Zn in preparation of ZnS). As can be observed from SEM images, the adoption of NaOH leads to the decrease of average diameter of ZnS nanoparticles from 1.5  $\mu\text{m}$  to around 20 nm (Fig. 1a, b). Significantly, the morphologies of Zn<sub>1-x</sub>Cd<sub>x</sub>S/CdS heterostructure samples were closely dependent on that of ZnS precursors: the heterostructure derived from the ZnS with smaller particle sizes shows the higher porous morphology. (Fig. 1c, d and Fig. S2).

Characterization of the phase structure via XRD patterns (Fig. 1e) indicates that the modulated morphology of heterostructure samples resulting from the different particle sizes of ZnS show tremendous effect on the crystallinity of the heterostructure. Compared with ZAC<sub>0</sub>, ZAC<sub>4</sub> possesses much stronger diffraction peaks corresponding to CdS and Zn<sub>1-x</sub>Cd<sub>x</sub>S phases due to its smaller particle size, and larger content of

heterostructure active sites confirmed by the largest amount of Cd from the electron dispersive X-ray spectrum (EDX) results (Fig. S3). The S, Zn and Cd distribute uniformly in the whole matrix of the nanoparticles (Fig. S4). Effect of the as-prepared heterostructure samples on their UV-Vis diffuse reflection spectra and band structure is displayed in Fig. 1f. Notably, the spectra of the heterostructure samples show two band edges, and the entire diffuse reflection spectra could be divided into region I and II, which are corresponding to absorption in the UV and visible regions, respectively.<sup>18</sup> Moreover, the heterostructure samples with smaller particle size possess the larger bandgap ( $E_g$ ) in the region II (inset of Fig. 1f), which may be attributed to the quantum effect of CdS.<sup>18</sup>

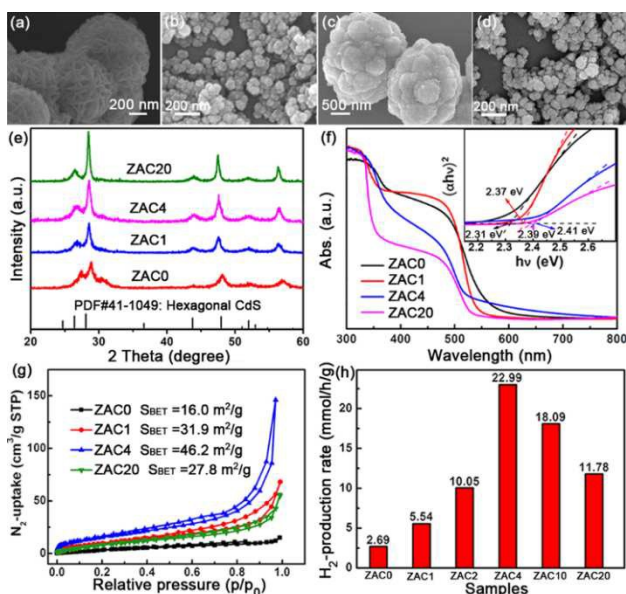


**Fig. 1** The SEM images of (a, b) ZnS prepared without NaOH and with NaOH (the molar ratio of NaOH/Zn equals 4), and (c, d) the corresponding heterojunction samples. The (e) XRD patterns, (f) UV-Visible diffuse reflection spectra and the corresponding  $(\alpha h\nu)^2$  versus  $h\nu$  curves (inset), and (g) nitrogen adsorption/desorption isotherms of the heterostructure samples with different particle sizes. (h) The H<sub>2</sub>-evolution rate of heterojunctions with different particle sizes.

A large surface area usually means more surface sites, which could facilitate the adsorption and reaction of reactants, and thus increase the photocatalytic activity due to the surface-based characteristic of photocatalytic water splitting reaction.<sup>23</sup> With decreasing their particle size, both ZnS and the relevant heterostructure show much larger nitrogen adsorption volumes and  $S_{BET}$  (Fig. S5) than those prepared without NaOH. Consequently, ZAC4 with the smallest particle size shows the largest nitrogen adsorption volume and  $S_{BET}$  among the ZACm samples (Fig. 1g). The HRTEM image of ZAC4 (Fig. S6) exhibits two lattice fringes with lattice constant of 0.334 and 0.207 nm, which corresponds to the Zn<sub>1-x</sub>Cd<sub>x</sub>S and CdS, respectively.

The photocatalytic H<sub>2</sub>-evolution activity of the heterostructure samples was performed in an aqueous solution containing 0.35 M Na<sub>2</sub>S and 0.25 M Na<sub>2</sub>SO<sub>3</sub> under visible light

irradiation ( $\lambda \geq 420$  nm) and compared in Fig. 1h. The decreased particle size in the ZACm samples results in the enhanced photocatalytic activity, and the maximum H<sub>2</sub>-evolution rate as high as 22.99 mmol/h/g was obtained in ZAC4. Whereas, a further increase of the content of NaOH leads to a slight reduction of the photocatalytic activity of the heterostructures due to their increased particle size. To validate the universality of this method, the ZnS/CuS heterostructures with modulated morphologies and the optimal Cu content were prepared by adopting ZnS with different particle sizes as precursors.<sup>24</sup> The ZnS/CuS derived from ZnS prepared with NaOH/Zn ratio of 4 shows much smaller particle size, larger nitrogen uptake and  $S_{BET}$ , and a much better photocatalytic activity under visible light (Fig. S7) than that of ZnS/CuS derived from ZnS prepared without NaOH.

On the basis of the investigation about the particle size-dependent photocatalytic activity, the optimal ZnS precursor with the smallest particle size was selected for further studying the effect of ZnO on the transfer efficiency of charge carriers and photocatalytic activity of the heterostructure. The different amounts of NaOH were adopted for the in-situ synthesis of the ZnO-embedded Zn<sub>1-x</sub>Cd<sub>x</sub>S/CdS heterostructures. The samples prepared with different NaOH/Cd<sup>2+</sup> molar ratios (labelled as n) were abbreviated as ZACAn (n = 0, 1, 5, 10, 15 and 20). Compared with ZACA0, the other ZACAn samples show much stronger diffraction peaks corresponding to the CdS phase, and the obvious diffraction peaks of ZnO were observed (Fig. 2). By comparison of UV-Visible diffuse reflection spectra of the ZACAn samples (Fig. S8), the adoption of NaOH during the reaction between ZnS and Cd<sup>2+</sup> shows no effect on the band structure of the heterostructure.

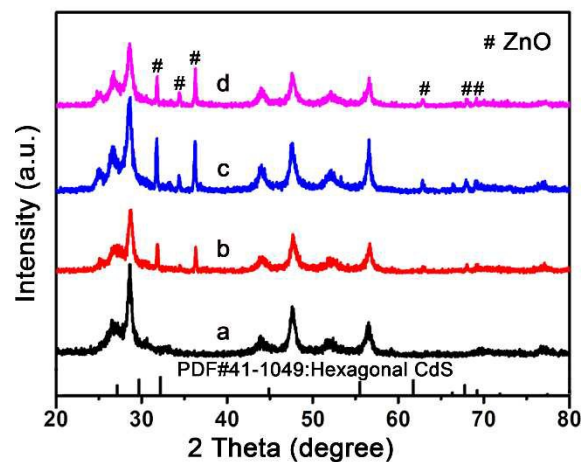


**Fig. 2** XRD patterns of the ZnO-embedded Zn<sub>1-x</sub>Cd<sub>x</sub>S/CdS heterostructure samples of (a) ZACA0, (b) ZACA1, (c) ZACA10 and (d) ZACA20.

Characterization of elements distribution by element mapping indicates that all the O, S, Zn and Cd elements were well-distributed in the skeleton of the heterostructure samples (Fig. 3a). As can be observed in the TEM image of ZACA10 (Fig. 3b), the nanoparticles show a uniform size distribution with an average diameter of around 20 nm. The ZnO-embedded

$Zn_{1-x}Cd_xS/CdS$  heterostructure was further confirmed by HRTEM (Fig. 3c). The lattice fringes corresponding to CdS, ZnO and  $Zn_{1-x}Cd_xS$  with well-defined heterostructure can be observed, and CdS quantum dots were loaded on the surface of the  $Zn_{1-x}Cd_xS$  nanoparticle core. Moreover, the ordered lattice fringes with the interplanar spacing of 0.282 nm, corresponding to the ZnO nanocrystals, can be observed at the edge of the  $Zn_{1-x}Cd_xS$  nanoparticle.

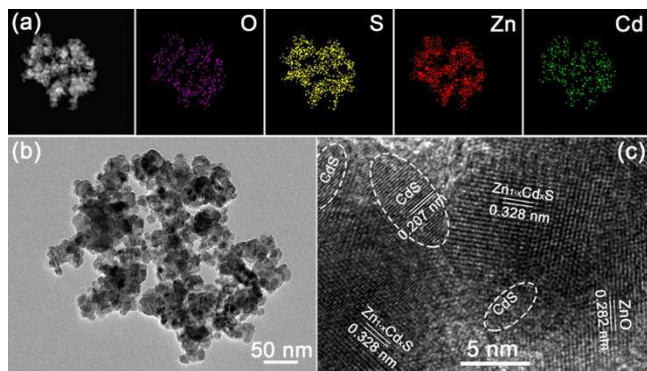


**Fig. 3** The (a) element mapping, (b) TEM and (c) HRTEM images of ZnO-embedded  $Zn_{1-x}Cd_xS/CdS$  heterostructure.

Effect of the ZnO nanocrystal on the photocatalytic activity of  $Zn_{1-x}Cd_xS/CdS$  heterostructure was compared in Fig. S9. The formation of ZnO in heterostructure could enhance its photocatalytic activity drastically, and ZACA10 possessing largest amount of ZnO shows the largest photocatalytic activity. Considering the similar microstructure morphology,  $S_{BET}$  (Fig. S10) and band structures of ZACA0 and ZACA10, the improved photocatalytic  $H_2$ -evolution rate from 22.99 mmol/h/g in ZACA0 (ZAC4) to 84.17 mmol/h/g in ZACA10 is mainly contributed from the formation of ZnO. This value is 765 times higher than that of CdS prepared by hydrothermal method, and is competitive in comparison with the previously reported CdS-based heterostructure (Table S1, supporting information).<sup>5, 18, 21, 25</sup> It is well known that the ZnO prepared by wet chemistry method at low temperature always possesses defect, such as oxygen vacancy, which may facilitate the charge separation and act as hydrogen production sites as reported in previous publications.<sup>26</sup> The oxygen vacancy in ZnO was confirmed by the Raman spectra (Fig. S11), where the peak located at around  $580\text{ cm}^{-1}$  was considered in connection with the oxygen vacancy in the ZnO crystal lattice.<sup>27</sup> Additionally, the ZnO-embedded heterostructure possesses excellent photocatalytic lifetime over 40 h (Fig. S12). Significantly, the photocatalytic stability of the ZnO-embedded  $Zn_{1-x}Cd_xS/CdS$  heterostructure was further confirmed by the unchanged phase structure of ZACA10 in XRD after the visible light irradiation for 40 h (Fig. S13), which indicates that the stable phase of ZnO loaded closely in the  $Zn_{1-x}Cd_xS/CdS$  skeleton even in dilute alkaline solution. The charge-carrier separation and transportation efficiencies were further approved via EIS spectra (Fig. S14). In accordance with the photocatalytic activity, ZACA10 shows the smallest semicircle in the middle-

frequency region, which indicates its fastest interfacial charge transmission.<sup>28</sup>

Since the sacrificial solution ( $Na_2S + Na_2SO_3$ ) for sulfide heterostructure is toxic and not stable during the practical application in air atmosphere, methanol has been employed as the sacrificial agent. The extremely important role of ZnO on the photocatalytic activity has been systematically investigated by comparing the photocatalytic  $H_2$ -production of ZnO-embedded  $Zn_{1-x}Cd_xS/CdS$  heterostructure (ZACA10) and the  $Zn_{1-x}Cd_xS/CdS$  heterostructure (ZACA0) in different reaction solutions as shown in Fig. 4a. As previously mentioned, the fine-grained  $Zn_{1-x}Cd_xS/CdS$  heterostructure possessed an excellent photocatalytic activity in the  $Na_2SO_3 + Na_2S$  solution, while shows a negligible photocatalytic  $H_2$ -evolution rate in methanol solution.<sup>16</sup> Unexpectedly, the presence of ZnO nanocrystals enhanced the photocatalytic activity obviously. Considering the oxidation process of sacrificial agents is complicated, and their oxidation dynamics should be different due to the different pH circumstances and oxidation process, sodium hydroxide has been added to the neutral methanol solution to obtain the similar alkalinity to that of  $Na_2SO_3 + Na_2S$  solution. And ZACA10 shows the photocatalytic activity in alkaline methanol solution of 55.22 mmol/h/g, which is very competitive in comparison with that in  $Na_2SO_3 + Na_2S$  solution (84.17 mmol/h/g). Whereas, ZACA0 still possesses a very low photocatalytic activity of only 2.35 mmol/h/g. The photocatalytic activity of ZACA10 is 23.48 times higher than that of ZACA0 in alkaline methanol solution, which is much larger than that (3.67 times) in  $Na_2SO_3 + Na_2S$  solutions. The tremendous distinction may be stemmed from the oxygen vacancy in ZnO, which could facilitate the separation of charge carriers, act as  $H_2$ -evolution sites and possess stronger oxidative capacity.

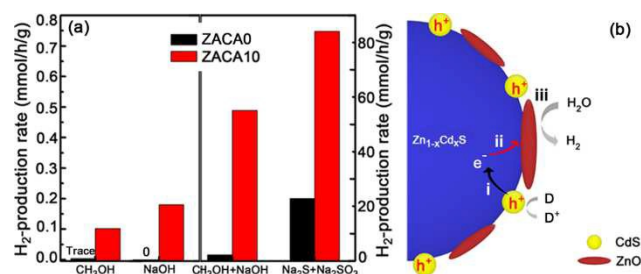


**Fig. 4** The (a) comparison results of the photocatalytic activity of ZACA0 and ZACA10 under visible light ( $\lambda \geq 420\text{ nm}$ ) with the different reaction solutions. The (b) charge carriers transport of ZnO-embedded  $Zn_{1-x}Cd_xS/CdS$  heterostructure.

To further investigate the role of ZnO in improving the photocatalytic activity of the  $Zn_{1-x}Cd_xS/CdS$  heterostructure, the alkaline solution with the same pH values to that of  $Na_2SO_3 + Na_2S$  solution has been used as reaction solution for evaluating the photocatalytic activities of ZACA0 and ZACA10.<sup>29</sup> Notably, in contrast to the no hydrogen evolution of ZACA0, ZACA10 gives a considerable photocatalytic activity of 0.18 mmol/h/g even in the absence of sacrificial agent. Considering their similar band structure and morphology, this qualitative change comes from the embedding of ZnO

nanocrystals in ZACA10. It is well known that the sacrificial agent plays a vital role in photocatalytic hydrogen evolution by consuming the photo-generated holes and facilitating separation of charge carriers. Consequently, in the absence of the hole scavenger,  $Zn_{1-x}Cd_xS/CdS$  heterostructure (ZACA0) without ZnO shows no hydrogen production. Thus, the presence of ZnO cocatalyst can facilitate the separation of charge carriers and act as the hydrogen production sites, and hence increase the hydrogen production even without sacrificial solution.<sup>30</sup> The transfer of the photo-generated charge carriers and electrons in the ZnO-embedded  $Zn_{1-x}Cd_xS/CdS$  heterostructure can be divided into three steps as shown in Fig. 4b. Under visible light irradiation, the photo-generated electrons transport from the conduction band (CB) of CdS to that of  $Zn_{1-x}Cd_xS$  as reported in previous publication,<sup>18</sup> while the photo-generated holes in the valence band (VB) of CdS can be consumed by sacrificial solution rapidly. In the second step, the electrons are further transferred to ZnO due to its wide  $E_g$ , where the electrons are trapped by the oxygen vacancies of ZnO.<sup>30</sup> Finally, the ZnO can act as reaction sites for reduction of proton and hydrogen production.

## Conclusions

In summary, the content of exposed active sites and morphology of  $Zn_{1-x}Cd_xS/CdS$  could be facilely modulated by the particle size of ZnS precursors. Simply increasing its content of active sites, the photocatalytic activity of the heterostructure increased 8.5-fold times in  $Na_2SO_3 + Na_2S$  solution. The photocatalytic  $H_2$ -production of  $Zn_{1-x}Cd_xS/CdS$  heterostructure can be further increased to 84.17 mmol/h/g by embedding ZnO as cocatalyst. Moreover, the existence of ZnO nanocrystal shows a competitive photocatalytic activity in methanol in comparison with that in  $Na_2S + Na_2SO_3$  solution under the similarly alkaline circumstance. More significantly, the ZnO-embedded  $Zn_{1-x}Cd_xS/CdS$  heterostructure gives considerable  $H_2$ -production even without sacrificial agent, although the  $Zn_{1-x}Cd_xS/CdS$  heterostructure shows no hydrogen evolution. This work not only introduces a facile surfactant-free hydrothermal route for increasing the content of exposed active sites in heterostructure, but also makes it possible for the improved photocatalytic activity of sulfide photocatalyst in eco-friendly sacrificial solution.

## Acknowledgements

This work was financially supported by NSFC (No. 21371099 and 21471080), the Jiangsu Specially-Appointed Professor, the NSF of Jiangsu Province of China (No. BK20130043 and BK20141445), the Natural Science Research of Jiangsu Higher Education Institutions of China (No. 13KJB150021), the Priority Academic Program Development of Jiangsu Higher Education Institutions, and the Foundation of Jiangsu Collaborative Innovation Center of Biomedical Functional Materials.

## Notes and references

Jiangsu Key Laboratory of Biofunctional Materials, College of Chemistry and Materials Science, Nanjing Normal University, Nanjing 210023, P. R. China. E-mail: yqlan@njnu.edu.cn; slli@njnu.edu.cn

†Electronic Supplementary Information (ESI) available: Figs and Tables. See DOI:10.1039/c000000x/

- (a) Q. Li, B. Guo, J. Yu, J. Ran, B. Zhang, H. Yan and J. R. Gong, *J. Am. Chem. Soc.*, 2011, **133**, 10878; (b) Z. Shen, G. Chen, Q. Wang, Y. Yu, C. Zhou and Y. Wang, *Nanoscale*, 2012, **4**, 2010; (c) F. Zuo, K. Bozhilov, R. J. Dillon, L. Wang, P. Smith, X. Zhao, C. Bardeen and P. Feng, *Angew. Chem., Int. Ed.*, 2012, **51**, 6223.
- X. Zhang, Y. Liu, S.-T. Lee, S. Yang and Z. Kang, *Energy Environ. Sci.*, 2014, **7**, 1409.
- D. Chen, F. Zhao, H. Qi, M. Rutherford and X. Peng, *Chem. Mater.*, 2010, **22**, 1437.
- Q. Xiang, B. Cheng and J. Yu, *Appl. Catal. B: Environ.*, 2013, **138–139**, 299.
- Y. P. Xie, Z. B. Yu, G. Liu, X. L. Ma and H.-M. Cheng, *Energy Environ. Sci.*, 2014, **7**, 1895.
- N. Bao, L. Shen, T. Takata and K. Domen, *Chem. Mater.*, 2008, **20**, 110.
- (a) X. Lai, J. E. Halpert and D. Wang, *Energy Environ. Sci.*, 2012, **5**, 5604; (b) L. Wang, H. Wei, Y. Fan, X. Liu and J. Zhan, *Nanoscale Res. Lett.*, 2009, **4**, 558
- H. McDaniel, M. Pelton, N. Oh and M. Shim, *J. Phys. Chem. Lett.*, 2012, **3**, 1094.
- X. Xu, L. Hu, N. Gao, S. Liu, S. Wageh, A. A. Al-Ghamdi, A. Alshahrie and X. Fang, *Adv. Funct. Mater.*, 2015, **25**, 445.
- (a) J. Ran, J. Zhang, J. Yu, M. Jaroniec and S. Z. Qiao, *Chem. Soc. Rev.*, 2014, **43**, 7787; (b) J.-H. Kang, S. H. Kim, M. Ebaid, J. K. Lee and S.-W. Ryu, *Acta Materialia*, 2014, **79**, 188; (c) Q. Xiang, J. Yu and M. Jaroniec, *J. Am. Chem. Soc.*, 2012, **134**, 6575.
- (a) C. Eley, T. Li, F. Liao, S. M. Fairclough, J. M. Smith, G. Smith and S. C. E. Tsang, *Angew. Chem., Int. Ed.*, 2014, **53**, 7838; (b) X. Wang, G. Liu, Z.-G. Chen, F. Li, L. Wang, G. Q. Lu and H.-M. Cheng, *Chem. Comm.*, 2009, 3452; (c) S. R. Lingampalli, U. K. Gautam and C. N. R. Rao, *Energy Environ. Sci.*, 2013, **6**, 3589; (d) Y. Tak, S. J. Hong, J. S. Lee and K. Yong, *J. Mater. Chem.*, 2009, **19**, 5945.
- (a) Y. Tang, H. Zhou, K. Zhang, J. Ding, T. Fan and D. Zhang, *Chem. Eng. J.*, 2015, **262**, 260; (b) C. Wang, D. Wu, P. Wang, Y. Ao, J. Hou and J. Qian, *Appl. Surf. Sci.*, 2015, **325**, 112.
- G. R. Li, T. Hu, G. L. Pan, T. Y. Yan, X. P. Gao and H. Y. Zhu, *J. Phys. Chem. C*, 2008, **112**, 11859.
- J. Hu, Y. Fan, Y. Pei, M. Qiao, K. Fan, X. Zhang and B. Zong, *ACS Catal.*, 2013, **3**, 2280.
- Z. Sun, H. Zheng, J. Li and P. Du, *Energy Environ. Sci.*, 2015, **8**, 2668.
- K. Wu, Z. Chen, H. Lv, H. Zhu, C. L. Hill and T. Lian, *J. Am. Chem. Soc.*, 2014, **136**, 7708.
- T.-T. Zhuang, Y. Liu, M. Sun, S.-L. Jiang, M.-W. Zhang, X.-C. Wang, Q. Zhang, J. Jiang and S.-H. Yu, *Angew. Chem., Int. Ed.*, 2015, **54**, 11495.
- J. Yu, J. Zhang and M. Jaroniec, *Green Chem.*, 2010, **12**, 1611.
- (a) Y. Yu, J. Zhang, X. Wu, W. Zhao and B. Zhang, *Angew. Chem., Int. Ed.*, 2012, **51**, 897; (b) Y. Huang, Y. Xu, J. Zhang, X. Yin, Y. Guo and B. Zhang, *J. Mater. Chem. A*, 2015, **3**, 19507.
- (a) J. Zhang, Z. Lin, Y. Lan, G. Ren, D. Chen, F. Huang and M. Hong, *J. Am. Chem. Soc.*, 2006, **128**, 12981; (b) D. Li, M. B. Muller, S. Gilje, R. B. Kaner and G. G. Wallace, *Nat. Nanotechnol.*, 2008, **3**, 101.

## Journal Name

- 21 K. Li, R. Chen, S.-L. Li, M. Han, S.-L. Xie, J.-C. Bao, Z.-H. Dai and Y.-Q. Lan, *Chem. Sci.*, 2015, **6**, 5263.
- 22 (a) X. Zou, P.-P. Wang, C. Li, J. Zhao, D. Wang, T. Asefa and G.-D. Li, *J. Mater. Chem. A*, 2014, **2**, 4682; (b) E. Mosayebi, S. Azizian and A. Hajian, *Superlattice. Microst.*, 2015, **81**, 226.
- 23 F. Chang, J. Luo, X. Wang, Y. Xie, B. Deng and X. Hu, *J. Colloid. Interf. Sci.*, 2015, **459**, 136.
- 24 J. Zhang, J. Yu, Y. Zhang, Q. Li and J. R. Gong, *Nano Lett.*, 2011, **11**, 4774.
- 25 (a) Q. Li, H. Meng, P. Zhou, Y. Zheng, J. Wang, J. Yu and J. Gong, *ACS Catal.*, 2013, **3**, 882; (b) G. Xin, B. Yu, Y. Xia, T. Hu, L. Liu and C. Li, *J. Phys. Chem. C*, 2014, **118**, 21928; (c) Q. Wang, J. Li, Y. Bai, J. Lian, H. Huang, Z. Li, Z. Lei and W. Shangguan, *Green Chem.*, 2014, **16**, 2728; (d) Z. Han, G. Chen, C. Li, Y. Yu and Y. Zhou, *J. Mater. Chem. A*, 2015, **3**, 1696; (e) J. Zhang, Y. Wang, J. Jin, J. Zhang, Z. Lin, F. Huang and J. Yu, *ACS Appl. Mater. Interfaces*, 2013, **5**, 10317; (f) L. Huang, X. Wang, J. Yang, G. Liu, J. Han and C. Li, *J. Phys. Chem. C*, 2013, **117**, 11584.
- 26 (a) H.-L. Guo, Q. Zhu, X.-L. Wu, Y.-F. Jiang, X. Xie and A.-W. Xu, *Nanoscale*, 2015, **7**, 7216; (b) B. Sambandam, R. J. V. Michael and P. T. Manoharan, *Nanoscale*, 2015, **7**, 13935.
- 27 (a) C. W. Zou, F. Liang and S. W. Xue, *Appl. Surf. Sci.*, 2015, **353**, 1061; (b) Q. Huang, T. X. Cun, W. B. Zuo and J. P. Liu, *Appl. Surf. Sci.*, 2015, **332**, 581; (c) Y. W. Tang, H. Zhou, K. Zhang, J. Ding, T. X. Fan and D. Zhang, *Chem. Eng. J.*, 2015, **262**, 260.
- 28 J. Zhang, J. Yu, M. Jaroniec and J. R. Gong, *Nano Lett.*, 2012, **12**, 4584.
- 29 (a) T. Simon, N. Bouchonville, M. J. Berr, A. Vaneski, A. Adrović, D. Volbers, R. Wyrwich, M. Döblinger, A. S. Sussha, A. L. Rogach, F. Jäckel, J. K. Stolarczyk and J. Feldmann, *Nat. Mater.*, 2014, **13**, 1013; (b) F. T. Wagner and G. A. Somorjai, *Nature*, 1980, **285**, 559.
- 30 S. Polarz, J. Strunk, V. Ischenko, M. W. E. van den Berg, O. Hinrichsen, M. Muhler and M. Driess, *Angew. Chem., Int. Ed.*, 2006, **45**, 2965.

# Graphical abstract

## In-situ synthesis of porous ZnO-embedded $\text{Zn}_{1-x}\text{Cd}_x\text{S}/\text{CdS}$

### heterostructure for the enhanced photocatalytic activity

Rong Chen, Kui Li, Xiao-Shu Zhu, Shuai-Lei Xie, Zhang-Long Dong, Shun-Li Li\* and Ya-Qian Lan\*

The in-situ embedding of ZnO cocatalyst on the fine-grained  $\text{Zn}_{1-x}\text{Cd}_x\text{S}/\text{CdS}$  heterostructure dramatically improves its photocatalytic activity even in the absence of hole scavenger, and makes the utilization of methanol solution as sacrificial agent for the sulfide semiconductor possible.

